REPORT

BIOMATERIALS

A bioinspired flexible organic artificial afferent nerve

Yeongin Kim,[1]* Alex Chortos,[2]* Wentao Xu,[3,4]*† Yuxin Liu,[5] Jin Young Oh,[6,7] Donghee Son,[6] Jiheong Kang,[6] Amir M. Foudeh,[6] Chenxin Zhu,[1] Yeongjun Lee,[3] Simiao Niu,[6] Jia Liu,[6] Raphael Pfattner,[6] Zhenan Bao,[6]† Tae-Woo Lee[3]†

The distributed network of receptors, neurons, and synapses in the somatosensory system efficiently processes complex tactile information. We used flexible organic electronics to mimic the functions of a sensory nerve. Our artificial afferent nerve collects pressure information (1 to 80 kilopascals) from clusters of pressure sensors, converts the pressure information into action potentials (0 to 100 hertz) by using ring oscillators, and integrates the action potentials from multiple ring oscillators with a synaptic transistor. Biomimetic hierarchical structures can detect movement of an object, combine simultaneous pressure inputs, and distinguish braille characters. Furthermore, we connected our artificial afferent nerve to motor nerves to construct a hybrid bioelectronic reflex arc to actuate muscles. Our system has potential applications in neurorobotics and neuroprosthetics.

Whereas classical von Neumann–based computing systems rely on centralized and sequential operations determined by a clock, neurons and synapses in biological nervous systems process information on the basis of distributed, parallel, and event-driven computation (*1*). As a result, classical systems exhibit the advantages of high speed and accuracy for well-defined problems, and biological systems are compact, fault tolerant, and power efficient for complex real-world problems, such as visual information processing, speech recognition, and movement control. Biological systems have influenced many fields of science and engineering, such as neuromorphic computing (*2*–*5*), bioinspired sensing systems (*6*–*9*), control theory for legged robots (*10*, *11*), and prosthetics (*12*–*14*).

Biologically inspired systems have been implemented at the software level in classical von Neumann–based systems to distinguish braille characters (*15*) and control actuators in legged robots (*10*, *11*). Alternatively, complex silicon circuits have been developed to mimic the spike-based information processing in biological systems, in which the function of a synapse was emulated by several conventional silicon transistors and a capacitor (*16*).

Device structures that emulate the functionality and signal processing of biological components may potentially simplify complex circuits by mimicking multiple synapses with a single device. Organic devices are attractive because their characteristics can be tuned through chemical design (*17*, *18*), they are compatible with printing methods that enable large-area coverage at a low cost (*13*), and they have relatively low elastic moduli, similar to those of soft biological systems.

The development of neuromorphic systems that mimic the sense of touch can benefit from the improved understanding of information processing in somatosensory peripheral nerves. The branched structure of slowly adapting type I (SA-I) afferent (sensory) neurons, which leads to a complex receptive field with many hotspots, is critical for sensing at a spatial resolution smaller than the spacing between the receptive field centers (fig. S1) (*19*), discerning the movement of objects, and distinguishing the orientation of edges on objects (*19*). The interneurons in the spinal cord have also been found to form synapses with multiple afferent neurons to encode and separate input features before tactile information is delivered to the cortex (*20*, *21*).

Here we describe an artificial afferent nerve based on flexible organic electronics (*22*–*25*). The bioinspired artificial afferent nerve emulates the functions of biological SA-I afferent nerves (Fig. 1A) by collecting data from multiple tactile receptors and conveying this information to biological efferent (motor) nerves, completing a hybrid bioelectronic reflex arc. Our artificial afferent nerve (Fig. 1, B and C, and fig. S2) consists of three core components: resistive pressure sensors, organic ring oscillators, and a synaptic transistor. Artificial mechanoreceptors consisting of a cluster of pressure sensors (each pressure sensor corresponds to a hotspot in the receptive field) are connected to an artificial nerve fiber (a ring oscillator) that converts external tactile stimuli into voltage pulses. The electrical signals from multiple artificial nerve fibers are then integrated and converted into postsynaptic currents by a synaptic transistor. The synaptic transistor can be subsequently used to interface with biological efferent nerves to form a complete monosynaptic reflex arc.

The resistive pressure sensors (*13*), with a sensitivity and working range comparable to those of biological receptors, are composed of a conducting pyramid-structured elastomer that forms a resistive pathway between CNT (carbon nanotube) and Au electrodes (Fig. 1B and fig. S3). An increase in pressure increases the contact area and therefore decreases the resistance between the CNT electrode and the Au electrodes (Fig. 2A).

The organic ring oscillator (figs. S4 and S5) was made of odd numbers of pseudo–complementary metal-oxide semiconductor (CMOS) inverters (figs. S6 and S7). The ring oscillator was designed to oscillate at frequencies that match the action potentials of sensory neurons (0 to 100 Hz) (supplementary text) (*26*). Frequency-encoded information can be more robust to voltage degradation and parasitic resistances than amplitude-encoded information. The supply voltage to the ring oscillator increased with the pressure on the sensor (Fig. 2A). The oscillation of the ring oscillator is "off" and the power consumption decreases (though not to 0 W because of the pseudo-CMOS design) when there is no pressure on the sensor. A constant nonzero pressure input leads to a fixed supply voltage to the ring oscillator, resulting in a constant frequency output that can be easily used to calculate the pressure input on the basis of a 1-to-1 relationship between pressure inputs and concurrent ring oscillator outputs, but this constant input also increases power consumption compared with that of biological SA-I afferent nerves, which have slow sensory adaption (supplementary text). An increase in pressure intensity resulted in an increase in both the frequency and the peak amplitude of electrical impulses from the oscillator (Fig. 2B). This is slightly different from the case in biology, in which the amplitudes of action potentials are usually the same (supplementary text).

The synaptic transistor (*17*, *27*, *28*) was fabricated with the use of a solution-processed conjugated polymer (the compound **P1**) (fig. S8B) as the hole-transporting semiconductor and an ion gel as the gate dielectric (figs. S8 to S11). Although the synaptic transistor was more limited in its capacity for run-time tuning of the temporal dynamics during operation (fig. S12) than the rather complex silicon synapse consisting of several transistors and a capacitor (*16*), we were able to obtain decay times for postsynaptic currents (typically 2 to 3 ms) (fig. S13) in a range comparable

[1]Department of Electrical Engineering, Stanford University, Stanford, CA, USA. [2]Department of Materials Science and Engineering, Stanford University, Stanford, CA, USA. [3]Department of Materials Science and Engineering, Seoul National University, Seoul, South Korea. [4]Institute of Photoelectronic Thin Film Devices and Technology, Nankai University, Tianjin, China. [5]Department of Bioengineering, Stanford University, Stanford, CA, USA. [6]Department of Chemical Engineering, Stanford University, Stanford, CA, USA. [7]Department of Chemical Engineering, Kyung Hee University, Yongin, South Korea.
*These authors contributed equally to this work.
†Corresponding author. Email: wentao@nankai.edu.cn (W.X.); zbao@stanford.edu (Z.B.); twlees@snu.ac.kr (T.-W.L.)

to that of decay times for synapses of biological afferent nerves (1.5 to 5 ms) (*21*, *29*) by choosing a specific polymer semiconductor during fabrication (table S1). The large variation in decay times within a material should have minimal effect on the output (*30*). The voltage outputs from the ring oscillators were connected to the gate electrodes of the synaptic transistor. The frequency of the current output from the synaptic transistor (Fig. 2C) matched the frequency of the voltage output from the ring oscillator (Fig. 2B). However, the pressure-current output from the synaptic transistor (Fig. 2C) was more linear than the pressure-voltage output of the ring oscillator (Fig. 2B). Our artificial afferent neuron consumes ~8 μW in the "off" state and ~25 μW in the "on" state (fig. S14). An array of our artificial afferent neurons can lead to a flexible artificial afferent nervous system—one of spiking neural networks (supplementary text)—with lower power consumption than the system consisting of a conventional flexible one-transistor–one-resistor pressure sensor array connected to Si-integrated circuit chips, which consume additional power for readout and control (fig. S15 and table S2).

Prolonged presynaptic voltage spikes can lead to more anion accumulation near or in the organic semiconductor and then increase the amplitude of postsynaptic currents (*31*). The peak postsynaptic currents are influenced by not only the magnitude of the pressure stimulus (Fig. 2, C and D) but also the duration of the pressure stimulus (Fig. 2, E and F). The duration of the pressure stimulus does not change voltage outputs from the ring oscillator. When we applied 500 cycles of 2-s pressure stimulation every 10 s (fig. S12), we detected slight increases in the postsynaptic currents and the decay times.

The synaptic transistor can combine signals from multiple ring oscillators because the ion gel allows the active channel to be gated by multiple electrodes (Fig. 3A and fig. S10C). The postsynaptic currents resulting from the pressures simultaneously applied to two pressure sensors (Fig. 3D) were comparable to the sum of the currents resulting from a pressure applied to two individual sensors (Fig. 3E = Fig. 3B + Fig. 3C). In the Fourier transform of each case (Fig. 3F), the synaptic transistor could combine signals from two pressure sensors and generate postsynaptic currents consisting of two frequency components corresponding to those from the two pressure sensors. Analogous to the way in which dendrites of a postsynaptic neuron in connection with a number of biological synapses add action potentials from multiple presynaptic neurons, a single synaptic transistor can add voltage inputs coming

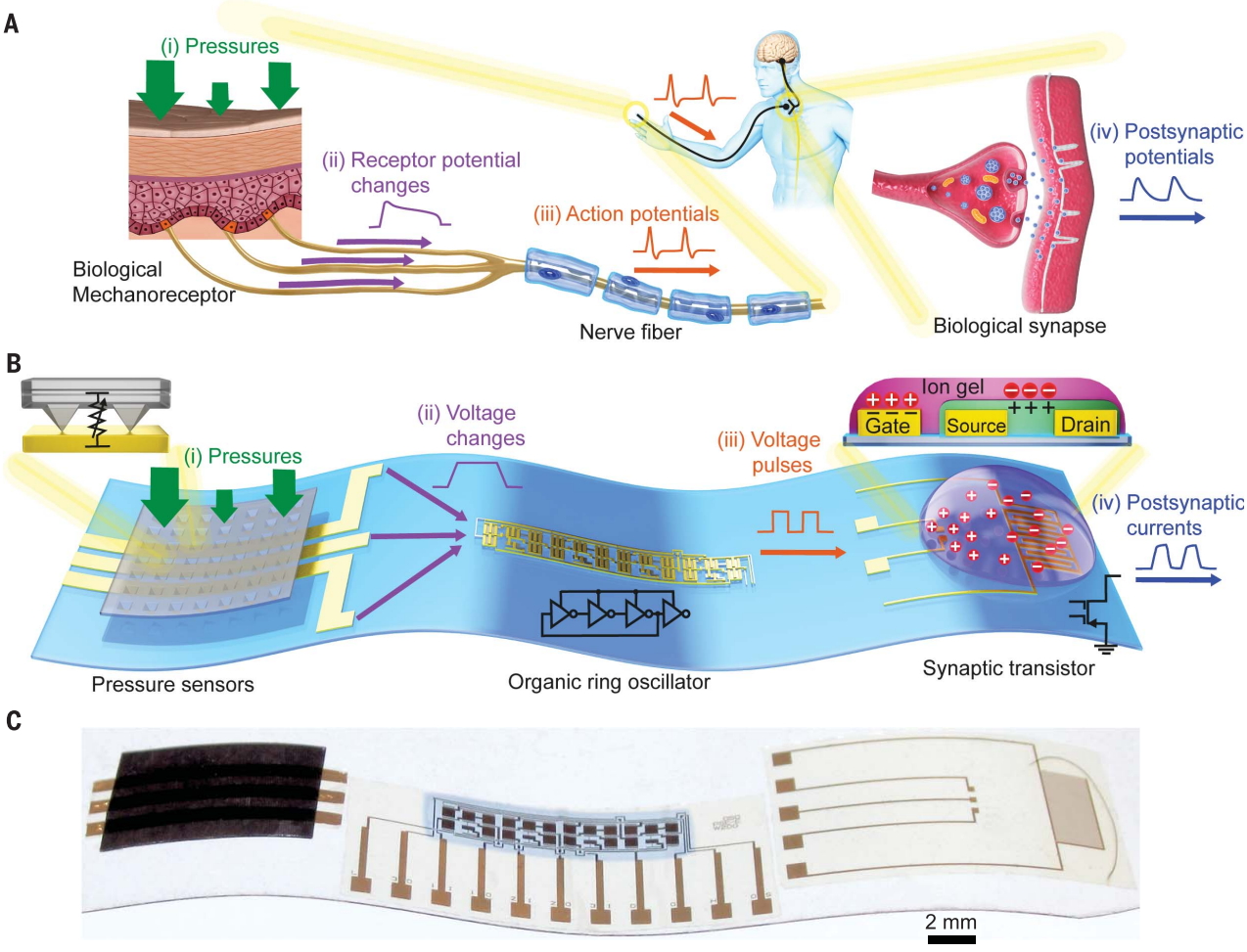

Fig. 1. An artificial afferent nerve system in comparison with a biological one. (**A**) A biological afferent nerve that is stimulated by pressure. Pressures applied onto mechanoreceptors change the receptor potential of each mechanoreceptor. The receptor potentials combine and initiate action potentials at the heminode. The nerve fiber forms synapses with interneurons in the spinal cord. Action potentials from multiple nerve fibers combine through synapses and contribute to information processing. (**B**) An artificial afferent nerve made of pressure sensors, an organic ring oscillator, and a synaptic transistor. Only one ring oscillator connected to a synaptic transistor is shown here for simplicity. However, multiple ring oscillators with clusters of pressure sensors can be connected to one synaptic transistor. The parts with the same colors in (A) and (B) correspond to each other. (**C**) A photograph of an artificial afferent nerve system.

from multiple ring oscillators. The synaptic transistor thus integrates signals more simply than the traditional synapse circuit made of several transistors and a capacitor, which needs separate circuits per input (*16*), although the decay time and the synaptic weight of each gate input in our synaptic transistor can be individually tuned only during fabrication, not during operation. Compared with uniformly applied pressures (80 kPa in fig. S16, D and F), pressures of different magnitudes (20 and 80 kPa in Fig. 3, D and F) led to different temporal and spectral patterns of postsynaptic currents. Such patterns could be used to encode information about large-scale textures measured by SA-I afferents.

One ring oscillator can combine signals from a cluster of pressure sensors, similar to a biological heminode (the beginning of the myelinated part of a nerve fiber) (*26*). When multiple pressure sensors are connected in parallel (Fig. 3G), the highest pressure will have a dominant effect on the output of the ring oscillator. This behavior mimics the branched structures and heminodes of afferent nerves that give rise to a sophisticated sense of touch in higher-order animals (*26*). A rodlike object was moved across two branches of pressure sensors in two different directions (Fig. 3G). When the object moved in the directions of the red and blue arrows, the postsynaptic current outputs had one valley corresponding to the object position between the two pressure sensors (Fig. 3H) and a monotonic increase without any local minimum (Fig. 3I), respectively. Analysis of the temporal profiles of postsynaptic currents in these two cases demonstrates the possibility of a bioinspired approach to recognize the direction and potentially the speed of object movement, which can be estimated from the duration of the valley of postsynaptic currents.

We used our artificial afferent nerves to identify braille characters pressed on an array of three pixels by two pixels (Fig. 3J and fig. S17). Six synaptic transistors accepted inputs from one oscillator, and 11 synaptic transistors each accepted inputs from two different oscillators. The peak frequencies of postsynaptic currents connected to one pixel (marked with a single number, from 1 to 6, and a blue box in fig. S17, A and B) are shown for all six pixels (Fig. 3K and fig. S18A). To quantify the difference in postsynaptic responses between different letters, we used Victor-Purpura spike train metrics (*32*) to calculate the Victor-Purpura distances (D_{VP}) between the characters (fig. S18, B and C). A larger D_{VP} means more dissimilarity between two spike trains. Compared with the smallest D_{VP} between different letters with the use of only pressure sensors and ring oscillators (i.e., without the signal integration of two pixels), the synaptic signal integration led to an increase in the smallest D_{VP} between different alphabets, which means that braille letters became more distinguishable because of the synaptic integration (Fig. 3L). Thus, this approach mimics the process of tactile information processing in a biological somatosensory system, where the signals of multiple tactile inputs from first-order neurons are integrated by synapses to partially process the information before delivery to the brain (*20*, *21*).

We connected our artificial afferent nerve to biological efferent nerves of a discoid cockroach (*Blaberus discoidalis*) (Fig. 4A) to complete a hybrid monosynaptic reflex arc (Fig. 4B), emulating a biological reflex arc (fig. S19). We used this hybrid system to demonstrate the flow of information from multiple pressure sensors through a neuromorphic circuit to deliver biomimetic postsynaptic oscillating signals into the biological efferent nerves in a detached cockroach leg (Fig. 4C), leading to the actuation of the tibial extensor muscle in the leg (Fig. 4D). The oscillating signals from our artificial afferent nerve elicit action potentials in nerves better than constant voltages (*33*). An increase in the amplitude and frequency of stimulation signals increases the number of activated muscle fibers and the forces generated by each muscle fiber, respectively (*33*, *34*). When we increased the intensity and

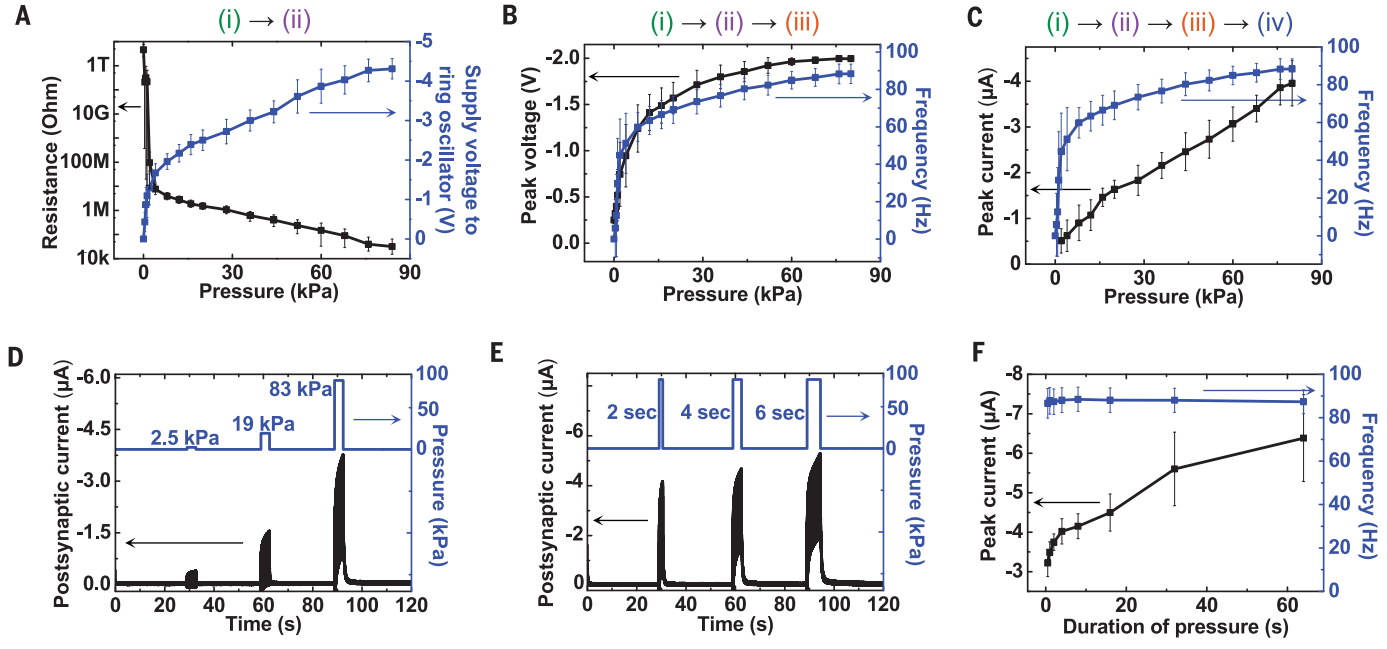

Fig. 2. Characteristics of an artificial afferent nerve system with one branch. (**A**) Resistance of a resistive pressure sensor and the corresponding change in the supply voltage of an organic ring oscillator in response to the change of pressure. The pressure sensor and the organic ring oscillator formed a voltage divider between a dc power supply voltage and the ground (fig. S2). (**B**) Peaks and oscillating frequencies of output voltages of ring oscillators as a function of pressures applied to pressure sensors. (**C**) Peak values and oscillating frequencies of postsynaptic currents of synaptic transistors depending on pressures. The gate voltage of the synaptic transistor was supplied from the ring oscillator output. (**D**) Postsynaptic current output of an artificial afferent nerve for three different pressure intensities. The duration of the stimulus application was 4 s for all three cases. (**E**) Response to three different durations of the pressure stimulus with a constant pressure intensity of 80 kPa. (**F**) The peak amplitude and frequency of the postsynaptic current depending on the duration of the stimulus application for the fixed amplitude of pressure (80 kPa). All error bars in (A) to (F) show 1 SD. (i) to (iv) correspond to the signals in Fig. 1. Arrows indicate the conversion of the signals by pressure sensors, organic ring oscillators, and synaptic transistors.

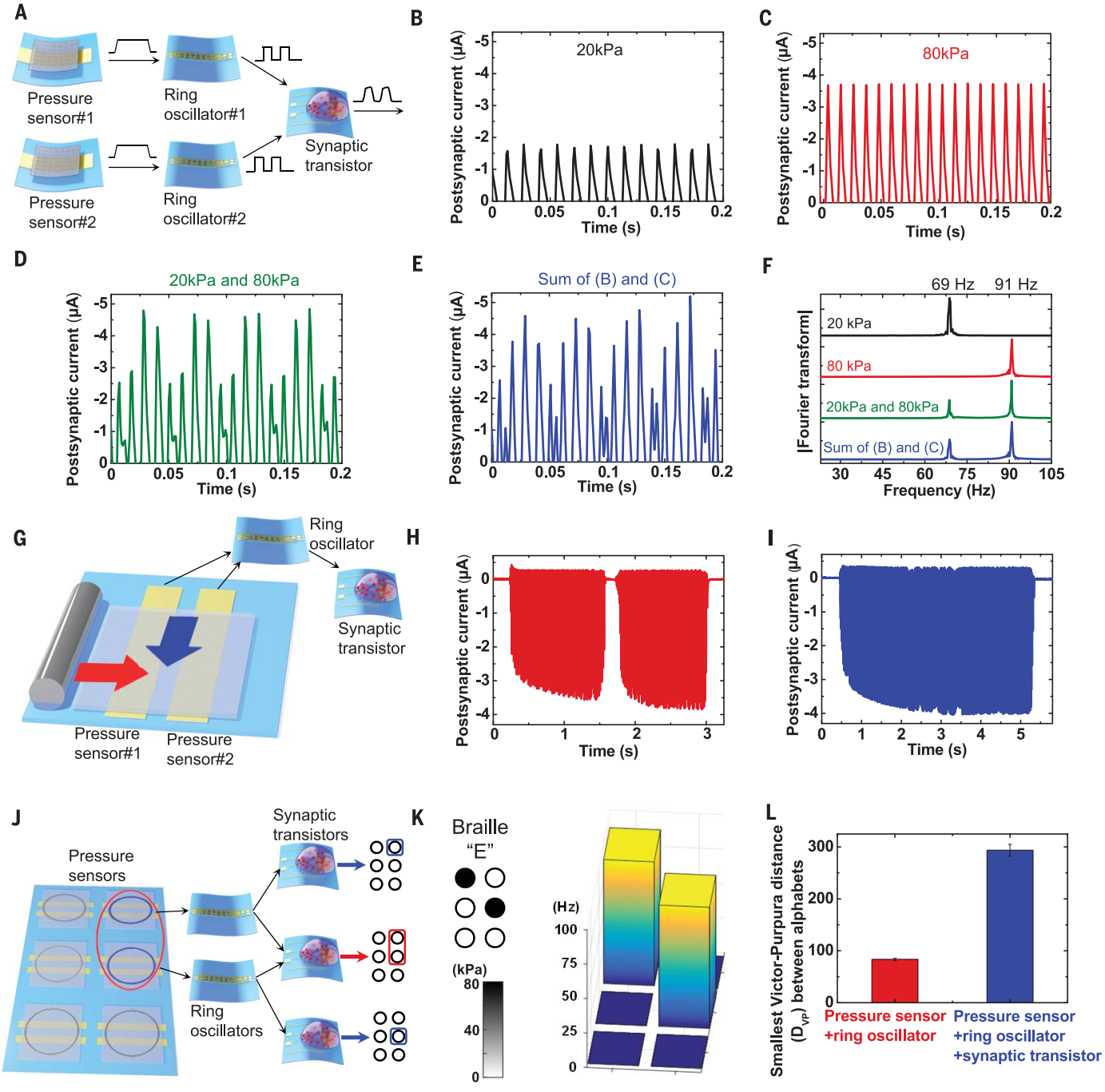

Fig. 3. Characterization of an artificial afferent nerve system with multiple branches. (**A**) Artificial afferent nerve with two branches of ring oscillators and pressure sensors measured in (B) to (F). (**B** and **C**) Postsynaptic currents when only one pressure sensor was pressed with 20 kPa (B) and 80 kPa (C), respectively. (**D**) Postsynaptic current when pressures of 20 and 80 kPa were simultaneously applied to two pressure sensors. (**E**) Plot of the sum of currents from (B) and (C). Our synaptic transistor functions as an adder so that (D) and (E) are almost the same. (**F**) The amplitude of Fourier transform of the cases in (B) to (E). Frequency components corresponding to pressures are maintained after the pressure information is combined by a synaptic transistor. Each transform was done for 4 s of data and normalized to its maximum peak. (**G**) Artificial afferent nerve with a cluster of two pressure sensors used for movement recognition in (H) and (I). The width of electrodes was 800 μm, and the distance between the two electrodes was 400 μm. (**H** and **I**) Postsynaptic currents when an object is moved in the direction of the red arrow (H) and the direction of the blue arrow (I) in (G). (**J**) Portion of the connections used for braille reading in (K) and (L). Ring oscillators and synaptic transistors were connected to an array of three pixels by two pixels of pressure sensors. A synaptic transistor was connected to either one or two ring oscillators. The complete combinations of connections used are shown in fig. S17, A and B. (**K**) (Left) Applied pressures on the pressure sensor array. (Right) Peak frequencies of postsynaptic currents from synaptic transistors connected to only one pixel (the synaptic transistors in blue boxes in fig. S17A). The results from all the braille characters are shown in fig. S18A. (**L**) The smallest Victor-Purpura distance (the metric used to quantify the difference between postsynaptic currents) between the postsynaptic currents of different alphabets. The integration of signals from two pixels by synaptic transistors improves the discrimination among the braille characters.

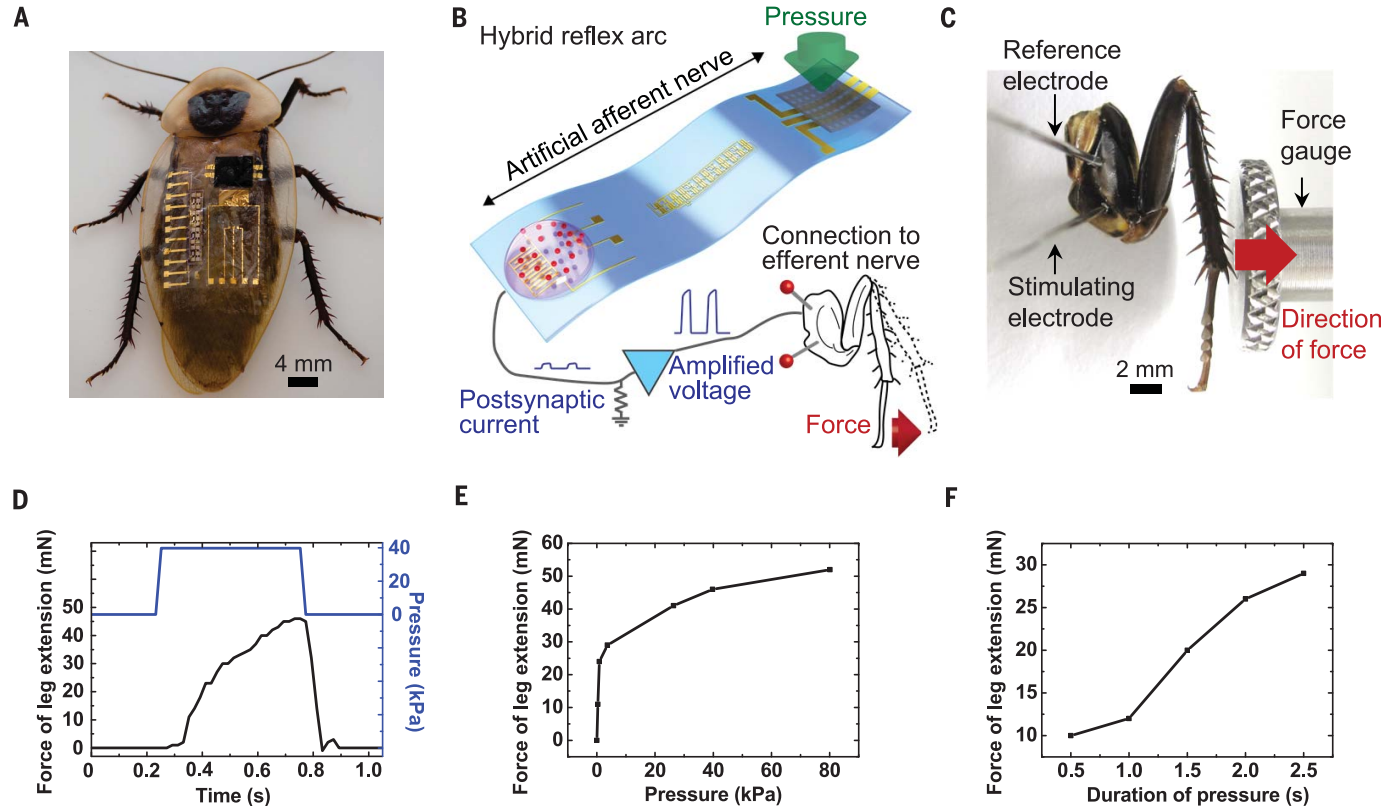

Fig. 4. Hybrid reflex arc. (**A**) Discoid cockroach with an artificial afferent nerve on its back. (**B**) Hybrid reflex arc made of an artificial afferent nerve and a biological efferent nerve. This experimental setup was used for measurements in (D) to (F). Pressure stimuli from multiple spots can be combined by an artificial afferent nerve and can be converted into postsynaptic currents. Postsynaptic currents are amplified to stimulate biological efferent nerves and muscles to initiate movement. (**C**) Photograph of reference and stimulating electrodes, a detached cockroach leg, and a force gauge used for (D) to (F). The tibial flexor muscle was dissected to remove its disturbance. (**D**) Isometric contraction force of the tibial extensor muscle in response to pressure on the artificial afferent nerve in (B). The pressure intensity and duration were 39.8 kPa and 0.5 s, respectively. (**E**) Summary of the maximum isometric contraction force of the tibial extensor muscle depending on the intensities of pressures. The duration of the stimulus application was 0.5 s for all measurements. (**F**) Effects of the duration of the pressure stimulus on the maximum isometric contraction force of the tibial extensor muscle. The amplitude of pressure was fixed at 360 Pa.

duration of the stimulus application on the artificial afferent nerve, the maximum isometric contraction force of the tibial extensor muscle increased accordingly (Fig. 4, E and F, respectively; additional data are in fig. S20). Isotonic contractions are shown in fig. S21 and movie S1.

Inspired by state-of-the-art understanding of biological afferent nerves, we fabricated an artificial afferent nerve based on organic devices that have multiple hotspots in the receptive field, generate action potentials depending on the combined pressure inputs, and integrate action potentials at a synaptic transistor. The biomimetic hierarchical structures were used to detect the shape and movement of an object in simple cases and to distinguish braille characters. Finally, our artificial afferent nerve was connected to biological efferent nerves to demonstrate a hybrid bioelectronic reflex arc and control biological muscles.

REFERENCES AND NOTES

1. S. Furber, *J. Neural Eng.* **13**, 051001 (2016).
2. S. B. Furber, F. Galluppi, S. Temple, L. A. Plana, *Proc. IEEE* **102**, 652–665 (2014).
3. J. Schemmel, D. Briiderle, A. Griibl, M. Hock, K. Meier, S. Millner, paper presented at the 2010 IEEE International Symposium on Circuits and Systems (ISCAS2010), Paris, France, 30 May to 2 June 2010.
4. N. Qiao *et al.*, *Front. Neurosci.* **9**, 141 (2015).
5. C. Mead, *Analog VLSI and Neural Systems* (Addison-Wesley Longman, 1989).
6. T. Delbrück, B. Linares-Barranco, E. Culurciello, C. Posch, paper presented at the 2010 IEEE International Symposium on Circuits and Systems (ISCAS2010), Paris, France, 30 May to 2 June 2010.
7. S.-C. Liu, A. Van Schaik, B. A. Mincti, T. Delbruck, paper presented at the 2010 IEEE International Symposium on Circuits and Systems (ISCAS2010), Paris, France, 30 May to 2 June 2010.
8. L. Osborn, R. Kaliki, A. Soares, N. Thakor, *IEEE Trans. Haptics* **9**, 196–206 (2016).
9. S. Caviglia, L. Pinna, M. Valle, C. Bartolozzi, paper presented at the 2016 IEEE International Symposium on Circuits and Systems (ISCAS2016), Montreal, QC, Canada, 22 to 25 May 2016.
10. R. D. Beer, R. D. Quinn, H. J. Chiel, R. E. Ritzmann, *Commun. ACM* **40**, 30–38 (1997).
11. D. Goldschmidt, F. Wörgötter, P. Manoonpong, *Front. Neurorobot.* **8**, 3 (2014).
12. K. A. Zaghloul, K. Boahen, *J. Neural Eng.* **3**, 257–267 (2006).
13. B. C.-K. Tee *et al.*, *Science* **350**, 313–316 (2015).
14. C. M. Oddo *et al.*, *eLife* **5**, e09148 (2016).
15. L. L. Bologna, J. Pinoteau, R. Brasselet, M. Maggiali, A. Arleo, *J. Physiol. (Paris)* **105**, 25–35 (2011).
16. C. Bartolozzi, G. Indiveri, *Neural Comput.* **19**, 2581–2603 (2007).
17. W. Xu, S.-Y. Min, H. Hwang, T.-W. Lee, *Sci. Adv.* **2**, e1501326 (2016).
18. Y. van de Burgt *et al.*, *Nat. Mater.* **16**, 414–418 (2017).
19. J. A. Pruszynski, R. S. Johansson, *Nat. Neurosci.* **17**, 1404–1409 (2014).
20. H. Jörntell *et al.*, *Neuron* **83**, 1444–1452 (2014).
21. F. Bengtsson, R. Brasselet, R. S. Johansson, A. Arleo, H. Jörntell, *PLOS ONE* **8**, e56630 (2013).
22. M. Park *et al.*, *Nat. Nanotechnol.* **7**, 803–809 (2012).
23. D. Khodagholy *et al.*, *Nat. Commun.* **4**, 1575 (2013).
24. D. T. Simon *et al.*, *Nat. Mater.* **8**, 742–746 (2009).
25. S. Lee *et al.*, *Nat. Nanotechnol.* **11**, 472–478 (2016).
26. D. R. Lesniak *et al.*, *eLife* **3**, e01488 (2014).
27. C. Qian *et al.*, *ACS Appl. Mater. Interfaces* **8**, 26169–26175 (2016).
28. J. Lee *et al.*, *J. Phys. Chem. C* **113**, 8972–8981 (2009).
29. Y. Takeuchi *et al.*, *J. Neurosci.* **32**, 6917–6930 (2012).
30. D. Querlioz, O. Bichler, C. Gamrat, paper presented at the 2011 International Joint Conference on Neural Networks (IJCNN), San Jose, CA, 31 July to 5 August 2011.
31. L. Herlogsson *et al.*, *Adv. Mater.* **19**, 97–101 (2007).
32. J. D. Victor, K. P. Purpura, *J. Neurophysiol.* **76**, 1310–1326 (1996).
33. J. Malmivuo, R. Plonsey, *Bioelectromagnetism: Principles and Applications of Bioelectric and Biomagnetic Fields* (Oxford Univ. Press, 1995).
34. J. W. S. Pringle, *J. Exp. Biol.* **16**, 220–231 (1939).

ACKNOWLEDGMENTS

We thank Y. Park, J. H. Jang, and J. Kim for theoretical background; J. Lopez for suggestions; and M. He for providing the conjugated polymer **P1**. **Funding:** This work was supported by a National Research Foundation of Korea (NRF) grant (NRF-2016R1A3B1908431) funded by the Korean government (Ministry of Science and ICT); the Center for Advanced Soft-Electronics, funded by the Ministry of Science and ICT as a Global Frontier Project (CASE-2013M3A6A5073175); and the Creative-Pioneering Researchers Program through Seoul National University (SNU). Research carried out at Stanford University is funded by Samsung Electronics. Y.Li. acknowledges NSS funding support from the Agency for Science, Technology and Research (A*STAR), Singapore. A.M.F. acknowledges postdoctoral fellowship support from the Natural Sciences and Engineering Research Council (NSERC) of Canada. R.P. acknowledges support from a Beatriu de Pinós fellowship (AGAUR 2014 BP-A 00094) from the Marie Curie Cofund. Part of this work was performed in the nano@Stanford labs (part of the National Nanotechnology Coordinated Infrastructure) and at the Stanford Nano Shared Facilities (SNSF), both of which are supported by the NSF under award ECCS-1542152. **Author contributions**: Y.K., A.C., W.X., Z.B., and T.-W.L. conceived of and designed the overall experiments. Y.K., A.C., and W.X. carried out experiments and collected related data. Y.Li. contributed to cockroach stimulation experiments. J.Y.O. helped fabricate pressure sensors. D.S. and A.M.F. aided in transfers of thin-film devices. J.K., Y.Le., and J.L. contributed to analyses of synaptic transistors. C.Z., S.N., and R.P. helped with electrical measurements. Z.B. and T.-W.L. initiated the study. Y.K., A.C., W.X., Z.B., and T.-W.L. analyzed all the data and cowrote the paper. All authors discussed the results and commented on the manuscript. **Competing interests:** Patents related to this work are planned. **Data and materials availability:** All data are available in the article or the supplementary materials.

SUPPLEMENTARY MATERIALS

www.sciencemag.org/content/360/6392/998/suppl/DC1
Materials and Methods
Supplementary Text
Figs. S1 to S21
Tables S1 and S2
References (*35*–*37*)
Movie S1

5 June 2017; accepted 18 April 2018
10.1126/science.aao0098

A bioinspired flexible organic artificial afferent nerve

Yeongin Kim, Alex Chortos, Wentao Xu, Yuxin Liu, Jin Young Oh, Donghee Son, Jiheong Kang, Amir M. Foudeh, Chenxin Zhu, Yeongjun Lee, Simiao Niu, Jia Liu, Raphael Pfattner, Zhenan Bao and Tae-Woo Lee

Science **360** (6392), 998-1003.
DOI: 10.1126/science.aao0098

I've got a feeling

Sensory (or afferent) nerves bring sensations of touch, pain, or temperature variation to the central nervous system and brain. Using the tools and materials of organic electronics, Kim *et al.* combined a pressure sensor, a ring oscillator, and an ion gel–gated transistor to form an artificial mechanoreceptor (see the Perspective by Bartolozzi). The combination allows for the sensing of multiple pressure inputs, which can be converted into a sensor signal and used to drive the motion of a cockroach leg in an oscillatory pattern.

Science, this issue p. 998; see also p. 966